

# The Spin Excitation Spectrum in Superconducting

## $\text{YBa}_2\text{Cu}_3\text{O}_{6.85}$

P. Bourges<sup>1</sup>, Y. Sidis<sup>1</sup>, H.F. Fong<sup>2</sup>, L.P. Regnault<sup>3</sup>, J. Bossy<sup>4</sup>, A. Ivanov<sup>5</sup>,  
B. Keimer<sup>2,6</sup>

*1 - Laboratoire Léon Brillouin, CEA-CNRS, CE Saclay, 91191 Gif sur Yvette, France*

*2 - Department of Physics, Princeton University, Princeton, NJ 08544, USA*

*3 - CEA Grenoble, Département de Recherche Fondamentale sur la matière Condensée,  
38054 Grenoble cedex 9, France*

*4 - CNRS-CRTBT, BP 166, 38042 Grenoble cedex 9, France*

*5 - Institut Laue-Langevin, 156X, 38042 Grenoble Cedex 9, France*

*6 - Max-Planck-Institut für Festkörperforschung, 70569 Stuttgart, Germany*

Science, **288** p 1234 (2000).

A comprehensive inelastic neutron scattering study of magnetic excitations in the near-optimally doped high-temperature superconductor  $\text{YBa}_2\text{Cu}_3\text{O}_{6.85}$  is presented. The spin correlations in the normal state are commensurate with the crystal lattice, and the intensity is peaked around the wave vector characterizing the antiferromagnetic state of the insulating precursor  $\text{YBa}_2\text{Cu}_3\text{O}_6$ . Profound modifications of the spin excitation spectrum appear abruptly below the superconducting transition temperature,  $T_C$ , where a commensurate resonant mode and a set of weaker incommensurate peaks develop. The data are consistent with models based on an underlying two-dimensional Fermi surface that predict a continuous, downward dispersion relation connecting the resonant mode and the incommensurate excitations. The magnetic incommensurability in the  $\text{YBa}_2\text{Cu}_3\text{O}_{6+x}$  system is thus not simply related to that of another high temperature superconductor,  $\text{La}_{2-x}\text{Sr}_x\text{CuO}_4$ , where incommensurate peaks persist well above  $T_C$ . The temperature dependent incommensurability is difficult to reconcile with interpretations based on charge stripe formation in  $\text{YBa}_2\text{Cu}_3\text{O}_{6+x}$  near optimum doping.

Electronic conduction in the high temperature superconductors cuprate takes place predominantly in  $\text{CuO}_2$  layers. Most theories therefore regard the electronic state that forms the basis of high temperature superconductivity as an essentially two-dimensional (2D) strongly correlated metal. The  $\text{CuO}_2$  sheets in one family of copper oxides ( $\text{La}_{2-x}\text{Sr}_x\text{CuO}_4$ ) have, however, been shown to be unstable against the formation of 1D “charge stripes”(1) even near doping levels where the superconducting transition temperature  $T_c$  is maximum. This observation has boosted models in which the underlying electronic instability is one-dimensional and the formation of (static or fluctuating) stripes is an essential precondition for high temperature superconductivity(2). However,  $\text{La}_{2-x}\text{Sr}_x\text{CuO}_4$  has some low energy phonon modes conducive to stripe formation that are not generic to the high- $T_c$  compounds, and the maximum  $T_c$  in this system is anomalously low. It is therefore important to test whether stripe based scenarios are viable in other cuprates with higher  $T_c$ , where this lattice dynamical peculiarity is not present.

The most salient signature of charge stripes is an associated (static or dynamic) spin density modulation that can be detected by neutron scattering. In  $\text{La}_{2-x}\text{Sr}_x\text{CuO}_4$  this modulation manifests itself as four well-defined incommensurate peaks at  $Q_\delta = (\pi(1 \pm \delta), \pi)$  and  $(\pi, \pi(1 \pm \delta))$  (in square lattice notation with unit lattice constant) in the magnetic spectrum, which are interpreted as arising from two 1D domains(3–6). Neutron scattering experiments on the  $\text{YBa}_2\text{Cu}_3\text{O}_{6+x}$  system have, however, revealed excitations that are peaked at  $Q_{AF} = (\pi, \pi)$ (7–13), the ordering wave vector of the 2D antiferromagnetic state observed when the doping level is reduced to zero. In particular, the commensurate “resonance peak” at  $Q = (\pi, \pi)$  that dominates the spectrum in the superconducting state(9–15), is difficult to reconcile with scenarios based on fluctuating 1D domains incommensurate with the host lattice. Recently, an incommensurate pattern with a four-fold symmetry reminiscent of  $\text{La}_{2-x}\text{Sr}_x\text{CuO}_4$  has also been discovered in some constant-energy cuts of the magnetic spectrum of underdoped  $\text{YBa}_2\text{Cu}_3\text{O}_{6.6}$ (16–18), which was taken as experimental sup-

port for stripe-based scenarios of superconductivity. We report a neutron scattering study of near-optimally doped  $\text{YBa}_2\text{Cu}_3\text{O}_{6.85}$  ( $T_c = 89\text{K}$ ) demonstrating that (unlike in  $\text{La}_{2-x}\text{Sr}_x\text{CuO}_4$ ) the incommensurate pattern appears only below  $T_c$ . Magnetic excitations in the normal state are commensurate and centered at  $Q = (\pi, \pi)$ . Our data are consistent with 2D Fermi liquid-like theories (not invoking stripes)(19–23), and especially that which predicts a continuous, downward dispersion of the magnetic resonance peak(20).

The experiments have been performed on a large twinned single crystal (mass  $\sim 9.5$  g) grown using the top seed melt texturing method(24). The sample was subsequently annealed in oxygen and displays a sharp superconducting transition ( $T_C$ ) at 89 K measured by a neutron de-polarization technique that is sensitive to the entire bulk(24). Experiments were carried out on two triple axis spectrometers: IN8 at the Institut Laue Langevin, Grenoble (France), and 2T at the Laboratoire Léon Brillouin, Saclay (France)(25). Two different scattering geometries were used on both spectrometers. On IN8, the (130) and (001) reciprocal directions were within the horizontal scattering plane. [We quote the wavevector  $\mathbf{Q}=(H,K,L)$  in units of the tetragonal reciprocal lattice vectors  $2\pi/a = 2\pi/b = 1.63 \text{ \AA}^{-1}$  and  $2\pi/c = 0.53 \text{ \AA}^{-1}$ ]. On 2T, an unconventional scattering geometry has been employed with the (100) and (011) reciprocal directions spanning the scattering plane. In both scattering geometries in-plane wavevectors equivalent to  $\equiv (\pi, \pi)$  can be reached, with an out-of-plane wave vector component close to the maximum of the structure factor of low energy excitations(24). In addition, wavevectors of the form  $\mathbf{Q} = (H, K, 1.7)$  around the antiferromagnetic wavevector were accessible on 2T by controlling the tilt angle, allowing a 2D mapping of the neutron intensity in the tetragonal basal momentum space and for a fixed energy transfer.

The magnetic resonance peak is observed at  $E_r = 41$  meV and  $Q = Q_{AF}$  in our sample(24) in agreement with previous reports for similar oxygen content(7,12). Here we present data obtained at energies below the resonance where the magnetic signal

is significantly weaker. Using established procedures, we use the temperature dependence of the magnetic intensity (which strongly decreases upon heating) to separate it from the phonon scattering that gradually increases with increasing temperature (Fig. 1A). Figs. 1B-D show constant-energy scans at  $E=35$  meV performed along the (130) direction (arrow in the inset of Fig. 1B). The phonon contribution has been subtracted for clarity. At low temperature, deep in the superconducting state, the magnetic scattering exhibits a double peak structure along  $(H, 3H, 0)$ . At 70 K, the intensity is still peaked at incommensurate wavevectors, but the discommensuration is slightly reduced. A single broad feature peaked at  $H=0.5$  is observed at 100 K in the normal state.

We have performed a comprehensive set of measurements in order to chart out in detail the spectral rearrangement indicated in Fig. 1. As an example, typical constant-energy scans were taken at low temperature along the  $H$  direction with  $K=1.5$  (Fig. 2A). The magnetic intensity is maximum at incommensurate wavevectors displaced from  $(0.5, 1.5)$  along  $H$ , and the incommensurability in this direction depends continuously on energy and forms a dispersing branch that closes at  $E_r$ . Accordingly, the maximum of the spin susceptibility at wave vector sufficiently far from  $(\pi, \pi)$  is shifted to lower energy than the resonant peak energy. The profile shapes are influenced by the instrumental resolution, and a deconvolution is required to accurately extract the peak positions. We found that a good global fit to the peak positions in both scattering geometries could be obtained by a convolution of the spectrometer resolution with the dispersion relation  $E = \sqrt{E_r^2 - (\alpha q)^2}$  with  $\alpha = (125 \pm 15)$  meV-Å(26). This downward dispersion (Fig. 2B) is shown along with the fitted peak positions. A neutron intensity map in the  $(H, K)$  reciprocal lattice plane measured at  $E=35$  meV and  $T=12$  K (not shown here) indicates that the intensity is not uniform along the dispersion surface. As in more underdoped samples(17,18), the intensity pattern has fourfold symmetry, with maxima shown as full squares in the inset of Fig. 1B. Although the data have not been analyzed in this manner, the

overall momentum dependence of the spin susceptibility reported in Fig. 3 below  $T_c$  is consistent with that reported in Refs.(16,18) as well as that in Refs.(10,15) where the incommensurability was not resolved.

Similar scans were repeated in the normal state (Fig. 3B) where the data thus far reported are inconclusive about the incommensurability. For all energies reported in Fig. 2, the normal state response can be systematically fitted by a single broad line (as shown at  $E=35$  meV in Fig. 1D). Fig. 3 shows that the momentum width at  $T=100$  K is energy independent up to 45 meV where the peaks begin to broaden(27). The  $q$ -width at low energy,  $\Delta_q = 0.21 \text{ \AA}^{-1}$  (HWHM) after deconvolution, agrees with previous reports for a similar oxygen content(15,28). Below  $T_c$ , the spin dynamics exhibit a more complex momentum dependence (Fig. 3A). While the momentum shape at energies above 45 meV is largely unaffected by superconductivity, there is a large increase in intensity and narrowing of the  $q$ -width at  $E_r = 41$  meV which is accompanied by a much weaker incommensurate response in a narrow energy range below  $E_r$ . Finally, the intensity is strongly reduced below 30 meV, which could result from the opening of a "spin-gap" below  $T_c$  as suggested by previous measurements(7,12).

The incommensurate response thus appears to be intimately linked to the occurrence of the resonance peak below  $T_c$ (7,9-14,24,29). In order to complete this picture, we now describe an accurate determination of the onset temperature of the incommensurate response and compare it to that of the resonance peak(8,10,11). The temperature dependence of the resonance intensity is reproduced for the present sample (Fig. 4A), and the raw neutron intensity (say without the phonon background subtracted) at the incommensurate position  $Q = (0.4, 1.5, 1.7)$  and  $E=35$  meV is shown versus temperature (Fig. 4B). Processed data at  $E=35$  meV (phonons subtracted and converted to absolute units(11,24)) are shown (Fig. 4C) a series of wavevectors (sketched by the open diamonds in Fig. 2B) spanning the locus of maximum intensity at low temperatures. Remarkably, all curves show a precipitous upturn at  $T_c$ , demonstrating clearly that both the resonance peak and the incommensurability are

induced by superconductivity. An indication of similar behavior had already been found in  $\text{YBa}_2\text{Cu}_3\text{O}_{6.7}$  ( $T_c=67$  K)(29) so that this behavior seems to be generic to the  $\text{YBa}_2\text{Cu}_3\text{O}_{6+x}$  superconductor.

Fig. 4C is also revealing in another respect. While all curves show the same sharp initial upturn below  $T_c$ ,  $\chi''(\mathbf{q}, 35 \text{ meV})$  generally goes through a maximum at a temperature  $T_m(\mathbf{q})$  that increases as  $\mathbf{q} \rightarrow (\pi, \pi)$ . A monotonic temperature dependence ( $T_m \rightarrow 0$ ) like the one of the resonance peak is seen only for  $\mathbf{q}$  close to the low temperature incommensurate wave vector determined above. However, the difference  $\chi''(T_m) - \chi''(T_c)$  is identical within the errors for the three  $\mathbf{q}$ -points away from  $(\pi, \pi)$ . This dramatic behavior can be straightforwardly understood as a consequence of the temperature (Fig. 1) and energy (Figs. 2 and 3) dependent incommensurability already indicated above. The resonance peak, together with the dispersion, forms quickly upon cooling below  $T_c$  and then sweeps sequentially through the wave vectors monitored in Figs. 4C.

In  $\text{YBa}_2\text{Cu}_3\text{O}_{6.85}$  the incommensurate response is part of a continuous dispersion below the resonance peak that is strongly renormalized upon approaching  $T_c$  and vanishes in the normal state. This is in stark contrast to the behavior reported for  $\text{La}_{2-x}\text{Sr}_x\text{CuO}_4$ (3–6) where no change of the peak position occurs across the superconducting temperature(3). Only around room temperature does the incommensurate structure begin to disappear(30). Further,  $\delta$  is energy-independent in  $\text{La}_{2-x}\text{Sr}_x\text{CuO}_4$ , but depends strongly on doping over a wide range of the phase diagram(6). Because of the energy dependence of  $\delta$  discussed above and the small number of samples investigated thus far, information about its doping dependence in  $\text{YBa}_2\text{Cu}_3\text{O}_{6+x}$  is still very incomplete. We note, however, that the discommensuration at  $E = 35 \text{ meV}$  ( $= E_r - 6 \text{ meV}$ ) we found in  $\text{YBa}_2\text{Cu}_3\text{O}_{6.85}$ ,  $\delta = 0.10 \text{ r.l.u.} \equiv 0.16 \text{ \AA}^{-1}$ , is equal to that reported in  $\text{YBa}_2\text{Cu}_3\text{O}_{6.6}$ (17) at  $E = 24.5 \text{ meV}$  ( $= E_r' - 9.5 \text{ meV}$  with  $E_r' = 34 \text{ meV}$ ) within the experimental error. Finally, the incommensurate fluctuations are only observed in a narrow energy range for fixed doping and are further substantially

weakened in fully oxidized  $\text{YBa}_2\text{Cu}_3\text{O}_7$ (9,10,12).

In the light of these observations, the analogy between the incommensurate spin excitations in  $\text{La}_{2-x}\text{Sr}_x\text{CuO}_4$  and  $\text{YBa}_2\text{Cu}_3\text{O}_{6+x}$  should not be overstated. Specifically, the interpretation in terms of stripe-domain fluctuations with a well-defined, doping dependent average periodicity, which is compelling and well documented in  $\text{La}_{2-x}\text{Sr}_x\text{CuO}_4$ , seems untenable in  $\text{YBa}_2\text{Cu}_3\text{O}_{6+x}$  near optimal doping. Our data indicate that the incommensurate excitations are continuously connected to the commensurate resonance peak by a dispersion relation with a negative curvature (Fig. 1B). The temperature dependence of Fig. 4 strongly supports a common origin of both phenomena. Some aspects of the behavior we observed have, in fact, been anticipated in the framework of microscopic models where the resonance peak is interpreted as a collective mode pulled below the gapped particle-hole spin-flip continuum(19–21). In particular, a downward dispersion has been predicted to arise naturally as a result of a momentum dependent pole in the spin susceptibility due to antiferromagnetic interactions(20). This picture also accounts for the rapidly diminishing intensity of the magnetic peaks away from  $(\pi, \pi)$ , as collective modes commonly lose oscillator strength upon approaching the continuum. Models based on dynamical nesting induced by a modification of the band dispersions(21–23) may also be consistent with our data. The models favored by our experimental results on near-optimally doped  $\text{YBa}_2\text{Cu}_3\text{O}_{6+x}$  are based on an interplay between band dispersions, Coulomb interactions and the  $d$ -wave gap function in a two-dimensional correlated electronic state.



## REFERENCES

1. J.M. Tranquada *et al.*, *Nature* **375**, 561 (1995).
2. See e.g. V.J. Emery, and S.A. Kivelson, *Physica C* **209**, 597 (1993).
3. T.E. Mason *et al.*, *Phys. Rev. Lett.* **68**, 1414 (1992).
4. T.R. Thurston *et al.*, *Phys. Rev. B* **46**, 9128 (1992).
5. S. Petit *et al.*, *Physica B* **234-236**, 800 (1997).
6. K. Yamada *et al.*, *Phys. Rev. B* **57**, 6165 (1998).
7. J. Rossat-Mignod *et al.*, *Physica C* **185-189**, 86 (1991).
8. H.A. Mook *et al.*, *Phys. Rev. Lett.* **70**, 3490 (1993).
9. H.F. Fong *et al.*, *Phys. Rev. Lett* **75**, 316 (1995).
10. P. Bourges, L.P. Regnault, Y. Sidis and C. Vettier, *Phys. Rev. B* **53**, 876 (1996).
11. H.F. Fong, B. Keimer, D. Reznik, D.M. Milius and I.A. Aksay, *Phys. Rev. B* **54**, 6708 (1996).
12. P. Bourges, in *The gap Symmetry and Fluctuations in High Temperature Superconductors*, J. Bok, G. Deutscher, D. Pavuna and S.A. Wolf Eds. (Plenum Press, 1998), pp. 349-371 (cond-mat/9901333).
13. L.P. Regnault, P. Bourges and P. Burllet in *Neutron Scattering in Layered Copper-Oxide Superconductors*, A. Furrer Ed. (Kluwer, Amsterdam, 1998), pp 85-134.
14. H.F. Fong, B. Keimer, F. Dogan and I.A. Aksay, *Phys. Rev. Lett.* **78**, 713 (1997).
15. P. Bourges *et al.*, *Europhys. Lett.* **38**, 313 (1997).
16. P. Dai *et al.*, *Phys. Rev. Lett.* **80**, 1738 (1998).
17. H.A. Mook *et al.*, *Nature* **395**, 580 (1998).

18. M. Arai *et al.*, *Phys. Rev. Lett.* **83** , 608 (1999).
19. D. van der Marel, *Phys. Rev. B* **51**, 1147 (1995).
20. F. Onufrieva and P. Pfeuty, preprint (cond-mat/9903097).
21. J. Brinckmann and P. Lee, *Phys. Rev. Lett.* **82**, 2915 (1999).
22. Y.-J. Kao, Q. Si and K. Levin, preprint (cond-mat/9908302)
23. K.-K. Voo and W.C. Wu, preprint (cond-mat/9911321).
24. H.F. Fong *et al.*, Accepted in *Phys. Rev. B.* (cond-mat/9910041).
25. On IN8, a Cu(111) monochromator and a pyrolytic graphite PG(002) analyzer, set at a fixed final energy of 35 meV, have been used. On 2T, PG(002) was employed as both monochromator and analyzer with a 14.7 meV fixed final energy. In both experiments, a PG filter was inserted into the scattered beam in order to remove higher order contamination. The sample was wrapped in aluminum foil and attached to the cold finger of a closed cycle helium refrigerator.
26. For a sake of simplicity, we describe the data with an isotropic dispersion relation ( $\alpha$  independent of  $q$ ). A slight anisotropy of  $\alpha$  between the (100) and (110) directions, with an associated intensity modulation, would reproduce the detailed momentum dependence reported in(17).
27. Above 45 meV, the magnetic peaks are characterized by broader response(18,24) reminiscent of the spin-waves of the undoped compound (See P. Bourges *et al.*, *Phys. Rev. B* **56**, R11439 (1997)).
28. A.V. Balatsky and P. Bourges, *Phys. Rev. Lett.* **82**, 5337 (1999).
29. P. Bourges *et al.*, in *High Temperature Superconductivity* S.E. Barnes *et al* Eds. (CP483 American Institute of Physics, Amsterdam, 1999) pp 207-212 (cond-mat/9902067).

30. G. Aeppli, *et al.*, *Science* **278**, 1432 (1997).

31. We wish to thank P. Baroni for his help during the experiment at LLB, and G. Aeppli, B. Hennion, G. Khaliullin, F. Onufrieva, and P. Pfeuty for stimulating discussions. The work at Princeton University was supported by the MRSEC program of the National Science Foundation under DMR- 9809483.

## FIGURES

FIG. 1. **(A)** Raw (uncorrected) room temperature scan which exhibits a phonon peak around  $H = 0.57$ . This scan displays none of the features of panels **(B-D)**. The inset in **(B)** is a sketch of the reciprocal space around the AF wavevector. The squares represent the locus of maximum magnetic intensity in the superconducting state. The arrow the represents the (130) direction of the scans. **(B-D)** Neutron intensity of constant-energy scans at  $E = 35$  meV performed along the (130) direction, with the room temperature scan subtracted: **(B)** I(11K)-I(300K) **(C)** I(70K)-I(300K) **(D)** I(100K)-I(300K). The momentum resolution was 0.03 r.l.u. ( $=0.15 \text{ \AA}^{-1}$ ) along (1,3,0) direction and  $0.3 \text{ \AA}^{-1}$  along the vertical direction. The energy resolution was 5 meV. We cannot rule out a small AF intensity ( $\sim 4$  times less than at 100 K) at room temperature.

FIG. 2. **(A)** Constant-energy scans performed along the  $H$  direction. The scans are offset by 120 counts from one another. The momentum resolution (FWHM) was 0.14 r.l.u. along  $H$  and 0.1 r.l.u. along  $K$ . The energy resolution was 4 meV. The lines are Gaussian displaced by  $\pm\delta H$  from  $Q_{AF}$ . The momentum transfer along  $c^*$  was fixed to the maximum of the magnetic structure factor,  $L = 1.7$ . The phonon background measured at room temperature has been subtracted from the data after proper correction for the Bose population factor<sup>(15)</sup>. **(B)** Dispersion of the incommensurate peaks observed in  $\text{YBCO}_{6.85}$ , deduced from (a) as described in the text. The square at  $H = 0.5$  represents the resonance peak,  $E_r=41$  meV. The other squares at  $0.5 \pm \Delta H$  come from the Gaussian fits shown in the lower panel. The open diamonds indicate the four wavevectors at  $E=35$  meV where the temperature dependence has been studied (see Fig. 4).

FIG. 3. Overall momentum dependence of the magnetic response in  $\text{YBCO}_{6.85}$  obtained **(A)** in the superconducting state at  $T=11$  K and **(B)** in the normal state at  $T=100$  K.

FIG. 4. **(A)** Temperature dependence of spin susceptibility in absolute units at the resonance energy  $E_r = 41$  meV. **(B)** Temperature dependence of the neutron intensity at  $E = 35$  meV and at the incommensurate wavevector  $Q_\delta = (1.5, 0.4, 1.7)$  (full circles). The open squares represent the background, determined by constant-energy scans (equivalent to the one shown in Fig. 2A). **(C)** Temperature dependence of spin susceptibility in absolute units at  $E = 35$  meV for 4 momentum transfers along  $a^*$  (4 open diamonds in Fig. 2B). The curves have been shifted by  $150 \mu_B^2/\text{eV}$  from one another. The susceptibility has been obtained by background subtraction and correction for the temperature factor  $1/(1 - \exp(-E/k_B T))$ . A marked change at  $T_c$  is observed at all wave vectors.

Fig 1:

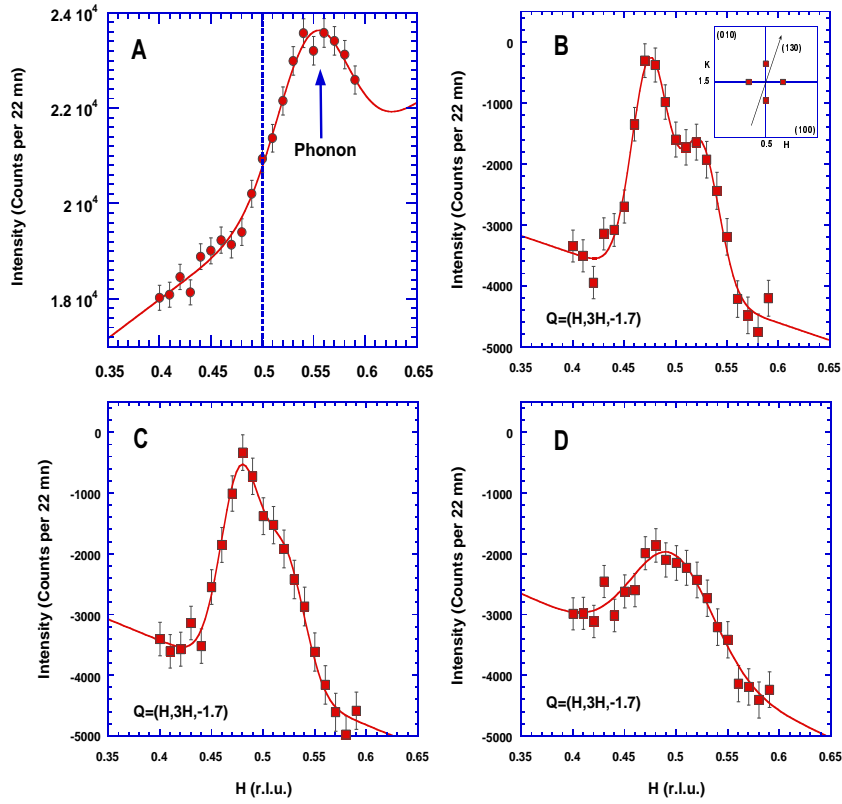


Fig 2:

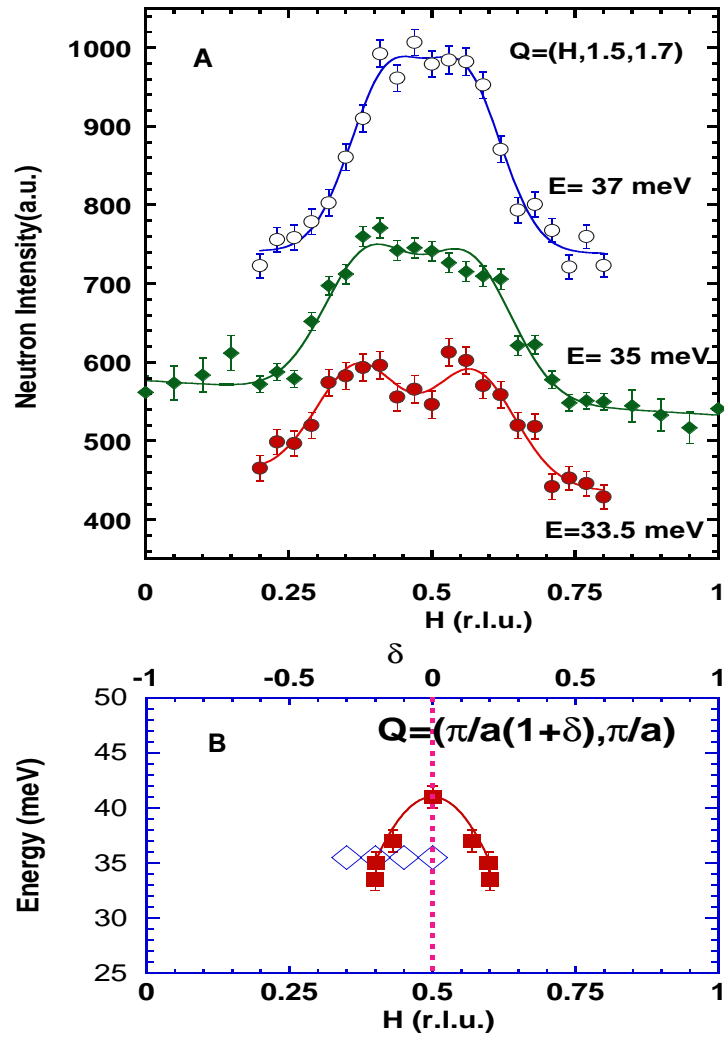


Fig 3:

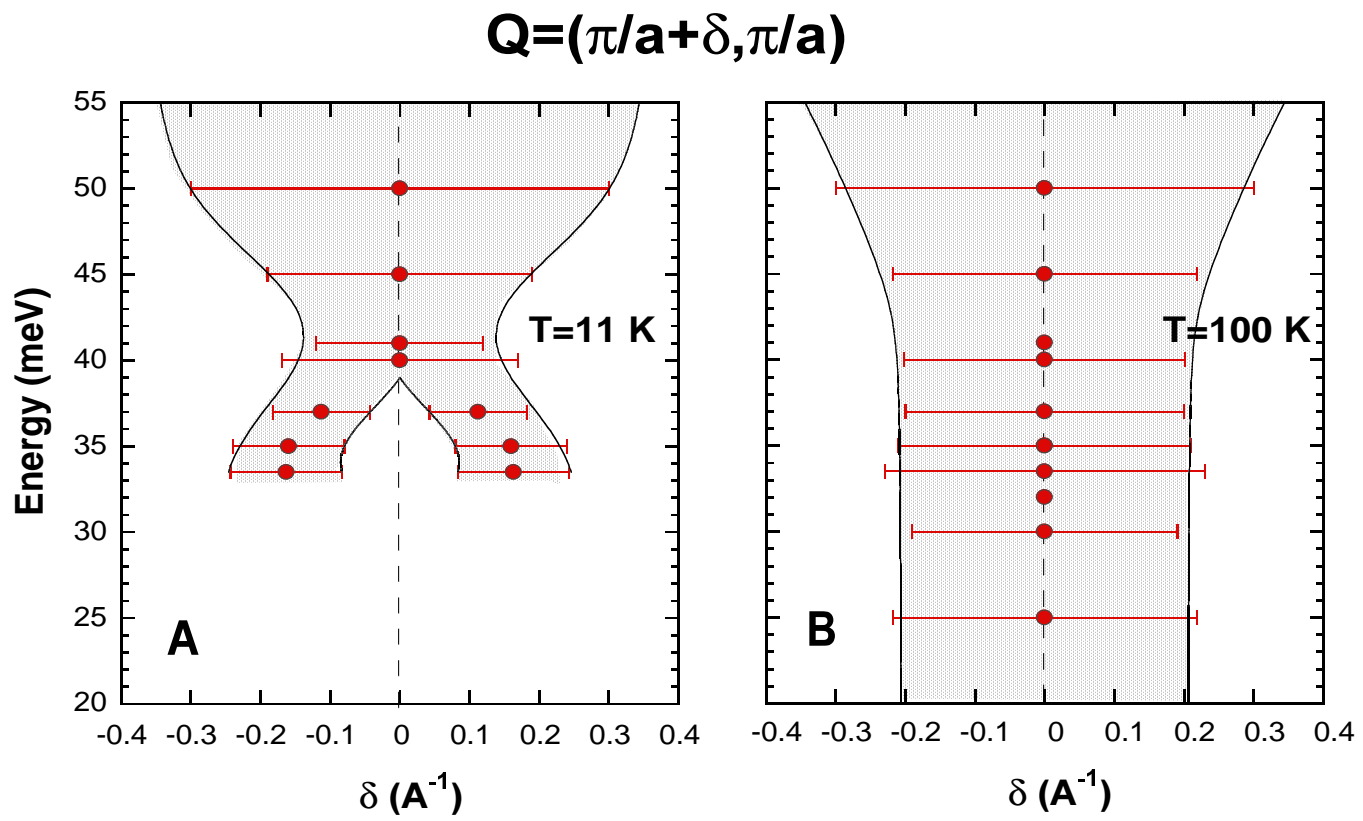




Fig 4:

